

# Improved online DMP spatial generalization and incorporation of dynamic via-points

Antonis Sidiropoulos<sup>1</sup> and Zoe Doulgeri<sup>1</sup>

**Abstract**—Dynamic Movement Primitives (DMP) have found remarkable applicability and success in various robotic tasks, which can be mainly attributed to their generalization, modulation and robustness properties. Nevertheless, the spatial generalization of DMP can be problematic in some cases, leading to excessive or unnatural spatial scaling. Moreover, incorporating intermediate points (via-points) to adjust the DMP trajectory, is not adequately addressed. In this work we propose an improved online spatial generalization, that remedies the shortcomings of the classical DMP generalization, and moreover allows the incorporation of dynamic via-points. This is achieved by designing an online adaptation scheme for the DMP weights which is proved to minimize the distance from the demonstrated acceleration profile in order to retain the shape of the demonstration, subject to dynamic via-point and initial/final state constraints. Extensive comparative simulations with the classical and other DMP variants are conducted, while experimental results validate the applicability and efficacy of the proposed method.

**Keywords**—Dynamic Movement Primitives, Programming by Demonstration

## I. INTRODUCTION

Dynamic Movement Primitives (DMP) [1], [2] have emerged as a promising method for encoding a desired trajectory and generalizing it to new situations. It is particularly favoured thanks to its ease of training, generalization, robustness and on-line modulation properties and has been applied in a plethora of practical robotic tasks and applications [3]–[7]. The trajectory to be encoded is typically provided through PbD (Programming by Demonstration) [8], as an intuitive and efficient means of teaching human-skills to robots.

In DMP, the objective of generalization is to generate a trajectory from a new initial position to a new, possibly time-varying, target position, while also preserving the shape of the demonstrated trajectory. To this end, different DMP variations and/or spatial generalization mechanisms have been proposed with the most well-known being the classical DMP formulation from [1]. However, the classical DMP spatial scaling has some important shortcomings, i.e. over-scaling of the generalized trajectory when the demonstrated end-points (initial and final position) are close, failure to generate a motion when the new end-points during execution coincide and mirroring of the trajectory when the sign of the difference between the new end-points is different from the sign of the difference of demonstrated ones. To remedy these issues, the

bio-inspired DMP formulation is proposed in [9]. Nevertheless, it exhibits poor generalization for targets that are not close to the demonstration, as highlighted in [10], where an improved version of the bio-inspired DMP is proposed to enhance its spatial generalization. A novel generalization to tackle the scaling issues of classical DMP is also proposed in [11]. While [10], [11] resolve the classical DMP scaling issues, they introduce over-scaling in trajectories with amplitudes bigger than the distance between the initial and final position, which is typical in many practical applications, like in packing applications where lifting an object and placing it down in a box is required. A different offline spatial generalization approach is proposed in [12] based on minimizing a norm, that is learned from multiple demonstrations, solving an iterative optimization problem.

Few DMP works consider via points on-line in their spatial generalization. Via-points can be particularly useful to adjust a trajectory on-line, e.g. to avoid obstacles in a predictable way by specifying through the via-points how the robot should circumvent them [13] or to push aside other objects that obstruct reaching pathways to a desired target [14]. Via-points are considered off-line in a DMP-like variant in [15] through offline optimization and in [16], which can include via-point constraints. So far, online incorporation of via-points is performed with probabilistic DMP [17], by online adapting the DMP weights to the new forcing term values, based on the provided via-points. Calculating the new forcing term value at via-points requires estimates of velocity and acceleration at the via-point, which can result in significant noise, that gets even more adverse, the sparser the via-points are arranged, as shown in [18]. Another approach to include via-points is proposed in [19], by introducing a time-varying attractor that shifts smoothly from one via-point to the next, until the final target [19]. Nevertheless, this does not ensure that the via-point will be reached and the distortions in the trajectory shape that this time-varying attractor incurs are not predictable.

Other movement primitives that can include via-points are the Probabilistic Movement Primitives (ProMP) [20], [21] and the Kernelized Movement Primitives (KMP) [22]. However, multiple demonstrations are required for training such primitives. Moreover, they cannot generalize well away from the demonstrations and have higher computational complexity with multiple DoFs. Of course, these primitives have other advantages compared to DMP and vice versa; choosing the most appropriate depends on the target application. In [13] the Via-point Movement Primitives (VMP) are introduced, that adopt ideas from DMP and ProMP, to achieve adaptation to via-points, and were shown to have better extrapolation

<sup>1</sup>Aristotle University of Thessaloniki, Department of Electrical and Computer Engineering, Thessaloniki 54124, Greece. antosidi@ece.auth.gr, doulgeri@ece.auth.gr

capabilities compared to ProMP, being also able to be trained from a single demonstration.

All aforementioned works are either off-line, or those that are online, consider static via-points, and do not address the case of via-points that may change dynamically. Dynamic changes of via-points occur if via-points are defined with respect to the position of the target or an obstacle, which is perturbed during execution. For instance in a human-robot collaborative packing scenario a via point may be defined on top of the target box which may be displaced by the human to a more ergonomic position for him. The robot has to adjust on-line to this change.

In this work we propose an improved online spatial generalization for DMP, that does not exhibit the shortcomings of the spatial scaling of the other DMP variants and can incorporate dynamic via-points. We achieve this by exploiting the novel DMP formulation presented in our previous work [23] to derive an online adaptation scheme for the DMP weights, based on minimizing the distance from the learned acceleration profile under the equality constraints of via-points. Moreover, we show how the proposed novel generalization can also be combined with our previous work [24] to impose kinematic inequality constraints in order to generate feasible trajectories in the presence of kinematic bounds related to the robot and the task environment (obstacles and via points). The combination of this work with [24] is showcased through simulations.

The rest of this paper is organized as follows: In Section II we provide the preliminaries for the novel DMP formulation from [23]. Section III is devoted to the proposed novel online generalization method. Simulations that demonstrate how the proposed method performs in comparison with the classical and other SoA DMP variants are provided in section IV. The practical usefulness and efficacy of the proposed method is further showcased in the experimental Section V. Finally, we draw the conclusions in Section VI. The source code for all conducted simulations and experiments can be found at [github.com/Slifer64/novel\\_dmp\\_generalization.git](https://github.com/Slifer64/novel_dmp_generalization.git).

## II. DMP PRELIMINARIES

In this section we briefly present the DMP formulation introduced in our previous work [23], which we exploit in this work to derive an improved on-line spatial generalization that can also incorporate dynamic via-points. As shown in [23], this formulation is mathematically equivalent to the classical DMP formulation from [1], retaining all properties of the latter.

Consider the state  $\mathbf{y} \in \mathbb{R}^n$ , which can be joint positions, Cartesian position or Cartesian orientation expressed using the quaternion logarithm (see Appendix A for preliminaries on unit quaternions). The DMP consists of two sets of differential equations, the transformation and the canonical system. A DMP can encode a desired trajectory  $t_j$ ,  $\mathbf{y}_{d,j}$  for  $j = 1 \dots m$  where  $m$  is the total number of points and  $T_{f,d} = t_m - t_1$  the time duration of the demo, and through its transformation system it can generalize this trajectory spatially from an initial position  $\mathbf{y}_0$  to a desired target position  $\mathbf{g}$ . Temporal scaling, i.e. execution of this trajectory with a different time duration or speed, is achieved through the canonical system, which

provides the clock  $s$  (time substitute) for the transformation system, to avoid direct time dependency. The **transformation system** is given by:

$$\ddot{\mathbf{y}} = \ddot{\mathbf{y}}_s - \mathbf{D}(\dot{\mathbf{y}} - \dot{\mathbf{y}}_s) - \mathbf{K}(\mathbf{y} - \mathbf{y}_s) \quad (1)$$

$$\mathbf{y}_s(s) = \mathbf{K}_s(\mathbf{f}_p(s) - \hat{\mathbf{y}}_{d,0}) + \mathbf{y}_0 \quad (2)$$

$$\mathbf{f}_p(s) = \mathbf{W}^T \boldsymbol{\phi}(s) \quad (3)$$

$$\mathbf{K}_s = \text{diag}((\mathbf{g} - \mathbf{y}_0) ./ (\hat{\mathbf{g}}_d - \hat{\mathbf{y}}_{d,0})) \quad (4)$$

with  $\mathbf{K}$ ,  $\mathbf{D} \in \mathcal{S}_{++}^n$ , with  $\mathcal{S}_{++}^n$  denoting symmetric  $n \times n$  positive definite gain matrices,  $\mathbf{y}_s$  is the scaled learned trajectory whose derivatives can be calculated analytically in closed form [23], matrix  $\mathbf{K}_s$  achieves the spatial scaling from the new initial position  $\mathbf{y}_0$  to a new target  $\mathbf{g}$ , while  $\hat{\mathbf{g}}_d \triangleq \mathbf{f}_p(s(T_{f,d}))$ ,  $\hat{\mathbf{y}}_{d,0} \triangleq \mathbf{f}_p(s(0))$  are the learned initial and target demo positions. The demonstrated position trajectory is encoded through the weighted sum of Gaussians in  $\mathbf{f}_p(s)$ , where the DMP weights  $\mathbf{W} \in \mathbb{R}^{K \times n}$  can be determined using Least Square, i.e.  $\min_{\mathbf{W}} \sum_{j=1}^m \|\mathbf{y}_{d,j} - \mathbf{W}^T \boldsymbol{\phi}_j\|_2^2$ , or Locally Weighted Regression (LWR) [1]. The Gaussian kernels are  $\boldsymbol{\phi}(s)^T = [\psi_1(s) \dots \psi_K(s)] / \sum_{i=1}^K \psi_i(s)$ , with  $\psi_i(s) = \exp(-h_i(s - c_i)^2)$  with  $c_i$  being the centers and  $h_i$  the inverse widths. A reasonable heuristic is to set the centers  $c_i$  equally spaced in  $[0, 1]$  and set  $h_i = 1/(a_h(c_{i+1} - c_i))^2$  where  $a_h$  controls the standard deviation of the Gaussian kernels. Choosing  $a_h \in [1.2, 1.5]$  produces empirically good approximation results.

Given  $s(0) \triangleq s_0$ ,  $s(\infty) \triangleq s_f$ , and considering without loss of generality  $s_0 = 0$  and  $s_f = 1$ , the **canonical system** is given by:

$$\ddot{s} = \begin{cases} d_1(\dot{s}_d - \dot{s}) & , s < s_f \\ -d_2\dot{s} - k_2(s - s_f) & , s \geq s_f \end{cases} \quad (5)$$

with  $d_1, d_2, k_2 > 0$ ,  $d_2 \geq 2\sqrt{k_2}$ ,  $s(0) = 0$  and  $\dot{s}(0) = \dot{s}_d = 1/T_f$ , where  $T_f$  is the desired motion duration. In the general case  $\dot{s}_d$  can also be time-varying. Notice that (5) guarantees phase  $s$  convergences from  $s(0) = 0$  to  $s \rightarrow 1$ ,  $\dot{s}, \ddot{s} \rightarrow 0$  as  $t \rightarrow \infty$ .

As shown in [23], the novel DMP formulation (1)-(4) is mathematically equivalent to the classical DMP. In particular, (1)-(4) can be mathematically manipulated to be written in a form similar to the classical one:

$$\dot{\mathbf{z}} = \mathbf{K}(\mathbf{g} - \mathbf{y}) - \mathbf{D}\mathbf{z} + (\mathbf{g} - \mathbf{y}_0)\mathbf{f}_s(s) \quad (6)$$

$$\dot{\mathbf{y}} = \mathbf{z} \quad (7)$$

$$\mathbf{f}_s(s) = \text{diag}(1./(\mathbf{g} - \mathbf{y}_0)) (\ddot{\mathbf{y}}_s + \mathbf{D}\dot{\mathbf{y}}_s - \mathbf{K}(\mathbf{g} - \mathbf{y}_s)) \quad (8)$$

The system is globally asymptotically stable at  $\mathbf{g}$ , since for  $t \rightarrow \infty$ ,  $\mathbf{f}_s \rightarrow \mathbf{0}$ , following from  $\dot{s}, \ddot{s} \rightarrow 0$  implying  $\ddot{\mathbf{y}}_s, \dot{\mathbf{y}}_s \rightarrow \mathbf{0}$  and  $s \rightarrow 1 \Rightarrow \mathbf{y}_s \rightarrow \mathbf{g}$ .

Spatial scaling is achieved through  $\mathbf{K}_s$  from (4) and temporal scaling by changing  $\dot{s}_d$  in (5). These are equivalent to changing  $\{\mathbf{g}, \mathbf{y}_0\}$  or the temporal scaling  $\tau$  according to  $\dot{\tau} = d_1(\tau_d - \tau)$  in the classical DMP [1], resulting in the exact same trajectory with the same spatial and temporal scaling [23].

Notice that to achieve temporal scaling, in contrast to the classical DMP formulation, there is no need to pre-multiply (6) - (7) by  $\tau$ , as this is handled by  $\dot{s}, \ddot{s}$  which are included in  $\dot{\mathbf{y}}_s, \ddot{\mathbf{y}}_s$  in  $\mathbf{f}_s(s)$  (this can be better understood by the mathematical equivalence analysis in [23]).

For encoding Cartesian orientation we can simply employ the quaternion logarithm, i.e. set  $\mathbf{y} = \log(\mathbf{Q} * \bar{\mathbf{Q}}_0)$  where  $\mathbf{Q} \in \mathbb{S}^3$  is the orientation as unit quaternion. We can then obtain the unit quaternion, rotational velocity and acceleration from  $\mathbf{y}$  and its derivatives using the mappings (20), (22) and (26) from Appendix A. Alternatively we can rewrite the transformation system as:

$$\dot{\omega} = \dot{\omega}_s - D(\omega - \omega_s) - K \log(\mathbf{Q} * \bar{\mathbf{Q}}_s) \quad (9)$$

where  $\mathbf{Q}_s, \omega_s$  and  $\dot{\omega}_s$  are obtained from (20), (22) and (26) from Appendix A using (2) and its analytically calculated derivatives.

### III. PROPOSED GENERALIZATION

Here we present a novel spatial generalization scheme that does not suffer from the drawbacks of the classical DMP generalization, reported in [9] and further allows the on-line incorporation of dynamic via-points<sup>1</sup>, while preserving the shape of the demonstrated trajectory, ensuring a smooth trajectory generation even for abrupt target or via-point changes. To this end, we remove the classical DMP scaling, by redefining (2) as

$$\mathbf{y}_s = \mathbf{f}_p(s) \quad (10)$$

and optimize the DMP weights so that the distance from the learned (from the demonstration) acceleration profile is minimized, while also satisfying the initial and final state constraints, i.e. start at  $t = 0$  from  $\mathbf{y}_0$  with zero velocity/acceleration and reach at  $t = T_f$  the target  $\mathbf{g}$ , again with zero velocity/acceleration. We assume that  $\mathbf{g}$  can change between 0 and  $T_f$  and is constant afterwards.

To achieve the novel spatial generalization and the incorporation of via-points, the following optimization problem has to be solved at each time-step  $i$ :

$$\min_{\mathbf{W}} \sum_{j=1}^m \left\| \frac{\partial^2 \hat{\mathbf{y}}_{d,j}}{\partial^2 s} - \mathbf{W}^T \frac{\partial^2 \phi_j}{\partial^2 s} \right\|_2^2 \quad (11a)$$

$$\text{s.t. } \mathbf{W}^T \mathbf{A}(0) = \mathbf{Y}_0 \quad (11b)$$

$$\mathbf{W}^T \mathbf{A}(1) = \mathbf{G}_i \quad (11c)$$

$$\mathbf{W}^T \Phi_{v,i} = \mathbf{Y}_{v,i} \quad (11d)$$

$$\mathbf{W}^T \mathbf{C}_j = \mathbf{Y}_j, \quad j = 1 \dots i \quad (11e)$$

where the learned acceleration profile is<sup>2</sup>  $\frac{\partial^2 \hat{\mathbf{y}}_{d,j}}{\partial^2 s} = \mathbf{W}_0^T \frac{\partial^2 \phi_j}{\partial^2 s}$  with  $\mathbf{W}_0 = \arg\min_{\mathbf{W}} J(\mathbf{W}^T \phi(s), \mathbf{y}_d)$ . The matrices in the first two equality constraints, (11b), (11c), with  $\mathbf{A}(s) = [\phi(s) \ \dot{\phi}(s) \ \ddot{\phi}(s)]$ , enforce the initial state  $\mathbf{Y}_0 = [\mathbf{y}_0 \ \mathbf{0}_{n \times 1} \ \mathbf{0}_{n \times 1}]$  and final state  $\mathbf{G}_i = [\mathbf{g}_i \ \mathbf{0}_{n \times 1} \ \mathbf{0}_{n \times 1}]$

<sup>1</sup>The term "point" can refer either to joint positions, Cartesian position, Cartesian orientation or Cartesian pose.

<sup>2</sup>Notice from (5) that, for nominal execution,  $\ddot{s} = 0$  and hence the acceleration, i.e. the 2nd time derivative of (2), is just  $\partial^2 \hat{\mathbf{y}}_{d,j} / \partial s^2$  scaled by the constant  $1/T_f^2$ .

conditions. Via-point constraints, which can be used to locally modify the DMP trajectory are defined in (11d), where  $\mathbf{Y}_{v,i} = [\mathbf{y}_{v,1} \dots \mathbf{y}_{v,L_i}]$  contains the via-points, with  $L_i$  their number at the current time-step  $i$ , and  $\Phi_{v,i} = [\phi(s_{v,1}) \dots \phi(s_{v,L_i})]$ .<sup>3</sup> The constraints in (11e) with  $\mathbf{C}_j = \mathbf{C}(s_j) = [\phi(s_j) \ \dot{\phi}(s_j) \ \ddot{\phi}(s_{j-1})]$  and  $\mathbf{Y}_j = [\mathbf{y}_j \ \dot{\mathbf{y}}_j \ \ddot{\mathbf{y}}_{j-1}]$  encode the current and all previous state constraints up to timestep  $i$ . The default option is to set  $\mathbf{Y}_j = \mathbf{W}_{i-1}^T \mathbf{C}_j$ . An alternative option is to set  $\mathbf{Y}_j$  to the actual robot's state at step  $j$  if it is also desirable to adapt online the DMP to changes of the robot's state induced by external signals, like measured forces. Regardless of the choice of  $\mathbf{Y}_j$ , the current state constraint for  $j = i$ , ensures that a smooth trajectory is generated by (1) even in the presence of abrupt target changes. The previous state constraints  $\mathbf{Y}_{1:i-1}$  guarantee that if the DMP is run in reverse as in [23], using the final adapted weights from the forward execution, the same trajectory (in reverse) will be executed. This could be expedient for safely retracting after the forward execution of a task, especially if the task has geometric constraints (like an insertion) which will have to be respected in the retraction phase.

#### A. Online DMP weights adaptation

Solving the problem in (11) on-line at each control cycle would be too slow and hence prohibitive for real-time usage. Instead we can employ the following recursive 2-step update at each time-step  $i > 0$ , which has computational complexity  $O(K^2)$  and can be carried out in real-time:

**step 1:** Remove the effect of the previous target  $\mathbf{g}_{i-1}$  and via-points:

$$\hat{\mathbf{W}}_i = \mathbf{W}_{i-1} + \hat{\mathbf{K}}_i (\hat{\mathbf{Z}}_i - \mathbf{W}_{i-1}^T \hat{\mathbf{H}}_i)^T \quad (12a)$$

$$\hat{\mathbf{P}}_i = \mathbf{P}_{i-1} - \hat{\mathbf{K}}_i \hat{\mathbf{H}}_i^T \mathbf{P}_{i-1} \quad (12b)$$

$$\hat{\mathbf{K}}_i = \mathbf{P}_{i-1} \hat{\mathbf{H}}_i (\hat{\mathbf{R}}_i + \hat{\mathbf{H}}_i^T \mathbf{P}_{i-1} \hat{\mathbf{H}}_i)^{-1} \quad (12c)$$

where

$$\hat{\mathbf{Z}}_i = [\mathbf{G}_{i-1} \ \mathbf{Y}_{v,i}^-], \quad \hat{\mathbf{H}}_i = [\mathbf{A}(1) \ \Phi_{v,i}^-], \quad \hat{\mathbf{R}}_i = -\epsilon \mathbf{I}_{3+b_i^-} \quad (13)$$

with  $\epsilon \approx 0^+$  and  $\mathbf{Y}_{v,i}^- \in \mathbb{R}^{n \times b_i^-}$  containing in columns the via-points that exist in the columns of  $\mathbf{Y}_{v,i-1}$  and not in  $\mathbf{Y}_{v,i}$  (i.e. are present at time-step  $i-1$  and not at  $i$ )<sup>4</sup> and  $\Phi_{v,i}^- = [\phi(s_k)]_{k=1:b_i^-}$  with  $s_k$  being the phase corresponding to each via-point in  $\mathbf{Y}_{v,i}^-$ .

**step 2:** Update to new target and via-points:

$$\mathbf{W}_i = \hat{\mathbf{W}}_i + \mathbf{K}_i (\mathbf{Z}_i - \hat{\mathbf{W}}_i^T \mathbf{H}_i)^T \quad (14a)$$

$$\mathbf{P}_i = \hat{\mathbf{P}}_i - \mathbf{K}_i \mathbf{H}_i^T \hat{\mathbf{P}}_i \quad (14b)$$

$$\mathbf{K}_i = \hat{\mathbf{P}}_i \mathbf{H}_i (\mathbf{R}_i + \mathbf{H}_i^T \hat{\mathbf{P}}_i \mathbf{H}_i)^{-1} \quad (14c)$$

where

$$\mathbf{Z}_i = [\mathbf{Y}_i \ \mathbf{G}_i \ \mathbf{Y}_{v,i}^+], \quad \mathbf{H}_i = [\mathbf{C}_i \ \mathbf{A}(1) \ \Phi_{v,i}^+], \quad \mathbf{R}_i = \epsilon \mathbf{I}_{6+b_i^+} \quad (15)$$

<sup>3</sup>If the phase  $s_{v,l}$ ,  $l = 1 \dots L_i$ , is not provided explicitly, a reasonable heuristic is to calculate it as  $s_v = \arg\min_{s_k} \|\mathbf{y}_s(s_k) - \mathbf{y}_v\|$ , where  $s_k$  in uniformly sampled in  $(s, 1]$ . Empirically, taking approximately 80 samples is sufficient, as the minimization need not be exact.

<sup>4</sup>Such is the case for instance if they are defined relative to a varying target or an object, whose position has changed or has been completely removed.

with  $\mathbf{Y}_{v,i}^+ \in \mathbb{R}^{n \times b_i^+}$  containing in columns the via-points that are present at time-step  $i$  and not at  $i-1$  and  $\Phi_{v,i}^+ = [\phi(s_k)]_{k=1:b_i^+}$  with  $s_k$  being the phase corresponding to each via-point in  $\mathbf{Y}_{v,i}^+$ .

For initialization at step  $i = 0$  we set  $\mathbf{Z}_0 = [\mathbf{Y}_0 \ \mathbf{G}_0]$ ,  $\mathbf{H}_0 = [\mathbf{A}(0) \ \mathbf{A}(1)]$ ,  $\mathbf{R}_0 = \epsilon \mathbf{I}_6$ ,  $\bar{\mathbf{W}}_0 = \mathbf{W}_0$  and  $\bar{\mathbf{P}}_0 = \mathbf{P}_0$  where

$$\mathbf{W}_0 = \operatorname{argmin}_{\mathbf{W}} J(\mathbf{W}^T \phi(x), \mathbf{y}_d), \quad \mathbf{P}_0 = \left( \sum_{j=1}^m \frac{\partial^2 \phi_j}{\partial^2 s} \frac{\partial^2 \phi_j}{\partial^2 s}^T \right)^{-1}$$

*Remark 1:* At the beginning of each execution, the DMP weights are initialized to the values that have been calculated offline once during the DMP training from the demonstration. Alternatively, if at a previous execution the DMP was modified, e.g. from via-points or the robot's actual state, resulting to some final weights  $\mathbf{W}_f$ , and it is desirable to retain this adjusted pattern at subsequent executions, one could set  $\mathbf{W}_0 = \mathbf{W}_f$ .

*Remark 2:* When  $\mathbf{g}$  is constant and/or we don't wish to adapt the DMP trajectory to via-points or changes of the actual robot's state, we can drop the constraints in (11d), (11e). It suffices to carry the above update only once at the beginning with  $\mathbf{Z}_0$ ,  $\mathbf{H}_0$  and  $\mathbf{R}_0$  to obtain  $\mathbf{W}_1$  and use  $\mathbf{W}_i = \mathbf{W}_1$  for  $i > 1$ .

*Remark 3:* In practice, due to finite numerical precision, setting  $\epsilon$  in  $\hat{\mathbf{R}}_i$ ,  $\mathbf{R}_i$  very close to zero can make the matrix being inverted in (12c) and (14c) ill-conditioned. We have found that in practice choosing  $\epsilon$  approximately in the range  $(10^{-10}, 10^{-6})$  does not create any numerical issues and the constraints are satisfied within an error tolerance of the order of  $10^{-4}$  or even less depending on how small  $\epsilon$  is.

*Remark 4:* Despite using the same value  $\epsilon$  in the above analysis for simplicity, it is easy to verify that different values of  $\epsilon$  can be chosen for each type of constraint. The selected  $\epsilon$  value can facilitate finding a solution in the optimization problem (11) in case constraints cannot be strictly satisfied (i.e. infinite accuracy). Then, the value of  $\epsilon$  essentially relaxes equality constraints, by penalizing the cost function (see *Theorem 3* from Appendix B). Choosing different values of  $\epsilon$  for each type of constraint, allows to prioritize which of these constraints should be satisfied with greater accuracy. Moreover, when adapting to the actual robot's state, which may be perturbed by noisy external signals, higher values of  $\epsilon$  can be used to suppress that noise.

*Remark 5:* The proposed recursive algorithm for updating the DMP weights to dynamically changing targets and/or via-points while ensuring a smooth trajectory generation can also be employed with different spatial scalings and cost functions. In particular, one can use these updates with  $\mathbf{y}_s$  as defined in (2), for any invertible matrix  $\mathbf{K}_s$ , just by replacing  $\mathbf{W}$  with  $\mathbf{K}_s \mathbf{W}$  and transforming each position  $\mathbf{y}$  (be it the current position, target, via-point etc.) according to  $\mathbf{y} := \mathbf{y} - \mathbf{y}_0 + \mathbf{K}_s \hat{\mathbf{y}}_{d,0}$ . Different objective functions can also be specified. E.g. it can be easily verified that optimizing the position (instead of the acceleration) results in the same equations with  $\mathbf{P}_0 = (\sum_{j=1}^m \phi_j \phi_j^T)^{-1}$ . More general objective

functions can also be specified, like the one from [12], which translates to defining  $\mathbf{P}_0 = \sum_{j=1}^m (\phi_j \mathbf{M} \phi_j^T)^{-1}$ , where  $\mathbf{M}$  is a metric matrix that is learned from multiple demonstrations.

## B. Derivation/Proof of the weights adaptation

In the following, we prove that (12), (14) solve the initial optimization problem given in (11). To this end, we will utilize the theorems provided in Appendix B. Problem (11) can be written compactly as:

$$\begin{aligned} \min_{\mathbf{W}} \operatorname{tr}\{(\ddot{\mathbf{Y}}_d - \mathbf{W}^T \ddot{\Phi})^T (\ddot{\mathbf{Y}}_d - \mathbf{W}^T \ddot{\Phi})\} \\ \text{s.t. } \mathbf{W}^T \bar{\mathbf{H}}_i = \bar{\mathbf{Z}}_i \end{aligned} \quad (16)$$

where  $\ddot{\mathbf{Y}}_d = [\frac{\partial^2 \hat{\mathbf{y}}_{d,1}}{\partial^2 s} \ \dots \ \frac{\partial^2 \hat{\mathbf{y}}_{d,m}}{\partial^2 s}] \in \mathbb{R}^{n \times m}$ ,  $\ddot{\Phi} = [\frac{\partial^2 \phi_1}{\partial^2 s} \ \dots \ \frac{\partial^2 \phi_m}{\partial^2 s}] \in \mathbb{R}^{K \times m}$ ,  $\bar{\mathbf{Z}}_i = [\mathbf{Y}_0 \ \mathbf{G}_i \ \mathbf{Y}_{1:i} \ \mathbf{Y}_{v,i}] \in \mathbb{R}^{n \times m_1}$  and  $\bar{\mathbf{H}}_i = [\mathbf{A}(0) \ \mathbf{A}(1) \ \mathbf{C}_{1:i} \ \Phi_{v,i}] \in \mathbb{R}^{K \times m_1}$  with  $m_1 = 6 + 3i + \bar{L}_i$ . Based on *Theorem 4* problem (16) is equivalent to:

$$\begin{aligned} \min_{\mathbf{W}} f_i(\mathbf{W}) \triangleq \operatorname{tr}\{(\ddot{\mathbf{Y}}_d - \mathbf{W}^T \ddot{\Phi})^T (\ddot{\mathbf{Y}}_d - \mathbf{W}^T \ddot{\Phi})\} \\ + \operatorname{tr}\{(\bar{\mathbf{Z}}_i - \mathbf{W}^T \bar{\mathbf{H}}_i)^T \bar{\mathbf{R}}_i^{-1} (\bar{\mathbf{Z}}_i - \mathbf{W}^T \bar{\mathbf{H}}_i)\} \end{aligned} \quad (17)$$

for  $\bar{\mathbf{R}}_i = \epsilon \mathbf{I}_{m_1}$ ,  $\epsilon \approx 0^+$ . Given now the solution at timestep  $i-1$  for problem (17) we want to find the solution for timestep  $i$ , for which the cost function can be written as:

$$f_i = \hat{f}_{i-1} + \operatorname{tr}\{(\mathbf{Z}_i - \mathbf{W}^T \mathbf{H}_i)^T \mathbf{R}_i^{-1} (\mathbf{Z}_i - \mathbf{W}^T \mathbf{H}_i)\}$$

where  $\hat{f}_{i-1} = f_{i-1} - \operatorname{tr}\{(\hat{\mathbf{Z}}_i - \mathbf{W}^T \hat{\mathbf{H}}_i)^T \hat{\mathbf{R}}_i^{-1} (\hat{\mathbf{Z}}_i - \mathbf{W}^T \hat{\mathbf{H}}_i)\}$ . Invoking *Theorem 5* the solution to  $\hat{f}_{i-1}$  is given by (12). Given now  $\hat{\mathbf{W}}_i, \hat{\mathbf{P}}_i$  for  $\hat{f}_{i-1}$  and using *Theorem 3* the solution to  $f_i$  is equivalent to the solution of  $\operatorname{tr}\{(\mathbf{W} - \hat{\mathbf{W}}_i)^T \hat{\mathbf{P}}_i (\mathbf{W} - \hat{\mathbf{W}}_i)\} + \operatorname{tr}\{(\mathbf{Z}_i - \mathbf{W}^T \mathbf{H}_i)^T \mathbf{R}_i^{-1} (\mathbf{Z}_i - \mathbf{W}^T \mathbf{H}_i)\}$ , which based on *Theorem 2* is given by (14).

## IV. SIMULATIONS

In the following we compare the DMP produced with the proposed spatial generalization, henceforth referred as DMP<sup>++</sup>, with the classical DMP, as well as other SoA variations that have been proposed in the literature. We further demonstrate and comment on the effects of adaptation to dynamic via-points and also including kinematic limits (inequality constraints) using the proposed generalization with [24]. Unless stated otherwise, in all cases, based on *Remark 4* and in the spirit that higher priority should be placed on the initial and final position constraints followed by the via-point constraints and then the previous state constraints, we chose  $\epsilon 10^{-9}$  for the initial and final position,  $10^{-7}$  for the initial and final velocity and acceleration constraints,  $10^{-7}$  for via-points and  $10^{-6}, 10^{-6}, 10^{-4}$ , for the previous state constraint. Notice that violation of the previous state constraint generates a discontinuous acceleration in the DMP (1), which will be larger the bigger the error in the equality constraint is.

### A. Spatial generalization comparison with classical DMP

We start off by examining the three basic cases where the classical DMP scaling is problematic [9]. For simplicity we consider an 1 DoF demonstration starting at position zero. Simulation results for each case are plotted in Fig. 1, where the demo is plotted with green dashed line, the proposed DMP<sup>++</sup> with blue and the classical DMP with magenta dotted line. In the first case (Fig. 1, top subplot) the demonstrated target  $g_d$  is quite close to the initial position  $y_{0,d} = 0$ . In this case, even a new target that is close to that of the demo, results in over-scaling for the classical DMP. In the figure, the resulting trajectory for the classical DMP is scaled by 400 for visualization purposes (the position actually converges to  $g$  but in the plot due to the scaling by 400 it is  $g/400 \approx 0$ ). In the second case (Fig. 1, middle subplot) the demo initial and target positions are different but the new target is the same with the initial position i.e.  $g = y_0$ . In this case, no motion is generated by the classical DMP. Finally, in the third case (Fig. 1, bottom subplot), if the new target is chosen below the initial position, or more generally when  $\text{sign}(g - y_0) = -\text{sign}(g_d - y_{0,d})$ , the classical DMP produces a mirrored trajectory. Unlike the classical DMP, the proposed DMP<sup>++</sup> retains the shape of the demonstrated trajectory in all cases, without exhibiting any side-effects.

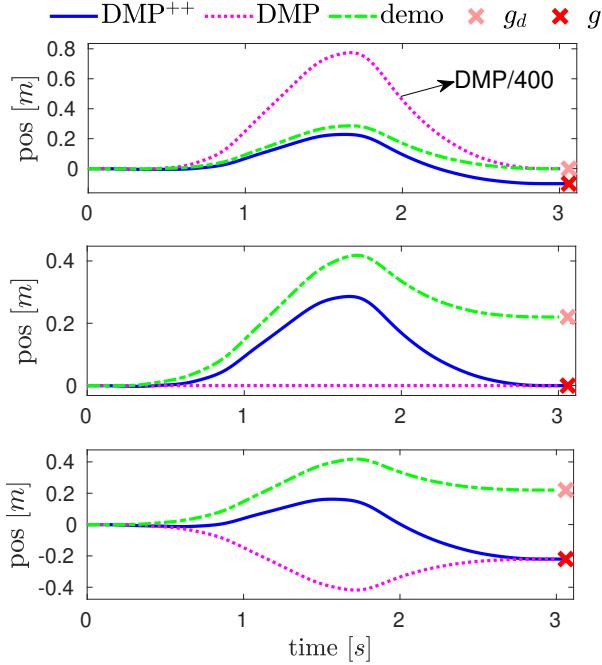


**Fig. 1:** Comparison with classical DMP generalization. Top: The demo start and goal positions are close. Middle: New goal set at the start position. Bottom: Mirroring.

### B. Spatial generalization comparison with other DMP variants

We further compare the proposed generalization against other SoA DMP variants that propose a different generalization. In particular, we compare against [11] (we will call it DMP-rot),

which proposes a different spatial scaling that remedies the 3 aforementioned drawbacks of classical DMP. We also compare against the bio-inspired DMP variant from [10] (we will call it DMP-bio<sup>+</sup>), which remedies the scaling problem of the bio-inspired DMP [9] for new target positions that are not close to the demo target position.

Notice that both [11], that assumes the classical DMP formulation, and [10], that assumes the bio-inspired DMP formulation, use for spatial generalization the scaling matrix  $K_s = R \frac{\|g - y_0\|}{\|g_d - y_{d,0}\|}$ , where  $R \in SO(3)$  is such that  $\frac{g - y_0}{\|g - y_0\|} = R \frac{g_d - y_{d,0}}{\|g_d - y_{d,0}\|}$ . It becomes obvious from such a  $K_s$ , and in particular from  $\frac{\|g - y_0\|}{\|g_d - y_{d,0}\|}$ , that displacement in one axis can affect the scaling in all axes, which in turn can result in over-amplification of the amplitude of an axis even if there is no displacement there. This effect is more pronounced for trajectories where in a specific axis the amplitude of the demo (i.e. the distance between the min and max position) is bigger than the distance between the original and final position. Such trajectories are typical in many real practical scenarios like packing.

To highlight these issues, we consider for the comparisons such a trajectory, with a higher amplitude than the distance between the initial and final demo position and examine the spatial generalization for 4 different displacements of the new target  $g$  from  $g_d$ . The results are plotted in Fig. 2, where each column depicts the results of a target displacement, with the 3D paths of each DMP variant on top and the corresponding velocities and acceleration of an indicative axis at the bottom. In the first case (Fig. 2-(a)), we can observe that although both  $g$  and  $g_d$  have the same  $z$ , the bigger displacement of  $g$  from  $y_0$  on the  $xy$  plane results in a large scaling for DMP-bio<sup>+</sup> and DMP-rot. This behaviour in practical pick and place tasks is arguably undesirable. For instance, when changing the  $xy$  position of a box where an object is to be placed, but the height of the box is the same, there is no good reason why the height of the DMP trajectory should alter. Moreover, this magnification of the amplitude generates much larger velocities and accelerations, as can be seen in the bottom subplots of 2-(a)<sup>5</sup>. In contrast, DMP<sup>++</sup> does not alter the amplitude of the trajectory and exhibits a behaviour close to the classical DMP. Notice also that the velocities and acceleration of DMP<sup>++</sup> and DMP coincide with the demo, as one would expect given that the height of the target is unaltered. Analogous conclusions can be drawn in 2-(b), where the height of the target is the same, but this time the displacement on the  $xy$  plane is smaller. Finally, in 2-(c),(d) the target is displaced in all axes, with lower or higher  $z$  respectively for  $g$ . Here, the scaling drawbacks of the classical DMP are clearly manifested. Notice also, that although DMP-rot and DMP-bio<sup>+</sup> do not generate large scalings and the resulting path retains the demo shape, it is nevertheless rotated in such a way that such a behaviour would not be very natural in practical tasks. (e.g. in a pick and place).

<sup>5</sup>Note that DMP-bio<sup>+</sup> produces a jerky acceleration which is owing to the use of the mollifier kernel which have finite support (instead of Gaussian kernels) [10].



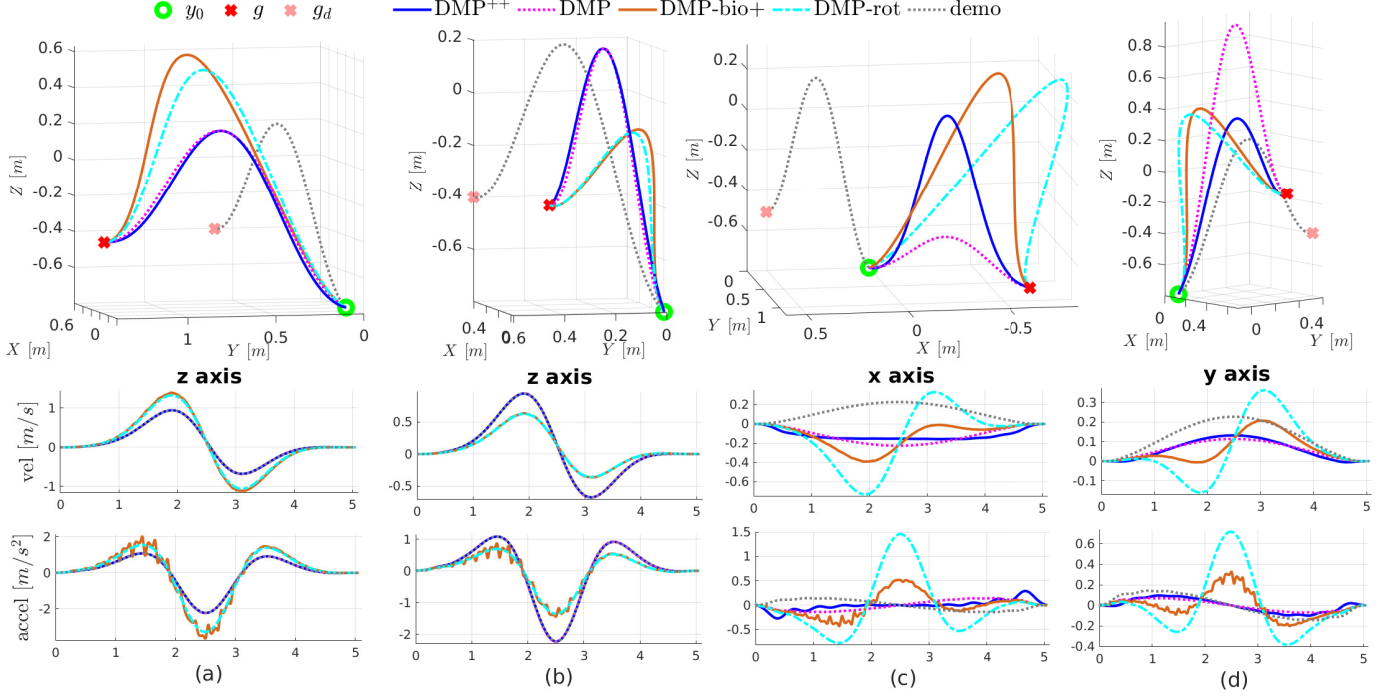


**Fig. 2:** Spatial generalization comparison between the proposed  $DMP^{++}$  and other DMP variants, for displacements of the new target  $\mathbf{g}$  different from the demo target  $\mathbf{g}_d$ . In each column the top subplot depicts the 3D paths and the two bottom subplots the corresponding velocities and accelerations for an indicative axis. (a)/(b): Same  $z$  and bigger/smaller displacement on the  $xy$  plane from  $\mathbf{y}_0$ . (c)/(d) Displacement in all 3 axis, with lower/higher  $z$ .

Nevertheless, it should be stressed that, while [11] and [10] have these drawbacks for trajectories where in a specific axis the amplitude of the demo (i.e. the distance between the min and max position) is bigger than the distance between the original and final position, they may still be applicable to reaching movements where the movement's amplitude is close to the distance between the start and final position. Moreover, they can presumably be more appropriate than  $DMP^{++}$  in very specific applications, e.g. drawing a shape, where it is desirable to have a spatial generalization that literally scales linearly the demo (through dilation in each axis separately as in [1] or using a rotation and dilation that accounts for all axes as in [11] and [10]).

### C. Generalization to dynamic via-points

Here we test the spatial generalization in the presence of dynamic via-points. We consider a single 2D demonstration for placing an object inside a box. During simulation we consider a tighter box that is also higher than that of the demonstration, hence via-points are used to ensure the proper placement inside the box. A rectangular obstacle is also present in the scene, with via-points specified relative to it, so as to ensure its avoidance in a predictable manner. To emulate dynamic changes in the scene, which typical occur in real environments, the position of the box and the target are displaced at different time instances.

We compare  $DMP^{++}$  with VMP [13]<sup>6</sup>. VMP are tested in

<sup>6</sup>Other methods like [25] and [10] are able to adapt only to a new continuous trajectory segment and not via-points. Also, ProMP [21] and KMP [22] require multiple demonstrations and do not address the case of dynamic via-points.

[13] only with static via-points, but can be easily adapted to dynamic via-points too. Specifically, a VMP is given by:

$$\mathbf{y}(s) = \mathbf{f}_p(s) + \mathbf{A}^T \phi_2(s) \quad (18)$$

where  $\mathbf{f}_p(s)$  is given by (3),  $\mathbf{A} \in \mathbb{R}^{6 \times n}$  contains in each column the coefficients of a 5th order polynomial for each DoF and  $\phi_2(s) = [1 \ s \ s^2 \ s^3 \ s^4 \ s^5]^T$ . The weights  $\mathbf{W}$  in  $\mathbf{f}_p$  are fitted to the demo, while  $\mathbf{A}$  is adapted according to the via-points, with the initial and target position treated as the first and final via-point. In particular, given the current phase value  $s$ , and the previous and next via-points  $\mathbf{y}_v(s_1)$ ,  $\mathbf{y}_v(s_2)$  with  $s_1 \leq s < s_2$ ,  $\mathbf{A}$  is determined by solving the system of equations:

$$\begin{bmatrix} \phi_2(s_j)^T \\ \dot{\phi}_2(s_j)^T \\ \ddot{\phi}_2(s_j)^T \end{bmatrix} \mathbf{A} = \begin{bmatrix} (\mathbf{y}_v(s_j) - \mathbf{f}_p(s_j))^T \\ (\dot{\mathbf{y}}_v(s_j) - \dot{\mathbf{f}}_p(s_j))^T \\ (\ddot{\mathbf{y}}_v(s_j) - \ddot{\mathbf{f}}_p(s_j))^T \end{bmatrix}, \quad j \in \{1, 2\}$$

Similar to [13], we set the velocity and acceleration at each via-point equal to that of the demonstration. Since via-points may alter on the fly, to ensure continuity we consider as the first via-point the current VMP point, i.e. we set  $s_1 = s$  and  $\mathbf{y}_v(s_1) = \mathbf{y}(s)$  (except for the initial via-point, which has position  $\mathbf{y}_0$ ). If the via-points are static, this approach generates the same trajectory as in [13], since once  $\mathbf{A}$  is adapted from a via-point  $\mathbf{y}_v(s_1)$  to a next via-point  $\mathbf{y}_v(s_2)$ , then continuously updating  $\mathbf{A}$  between  $\mathbf{y}_v(s) = \mathbf{y}(s)$  and  $\mathbf{y}_v(s_2)$ , with  $s \in (s_1, s_2)$  obviously yields the same  $\mathbf{A}$ .

The simulated scenario and the results with  $DMP^{++}$  are depicted in Fig. 3. At the top subplot, the initial target and obstacle are shown, with the predicted DMP trajectory (i.e.

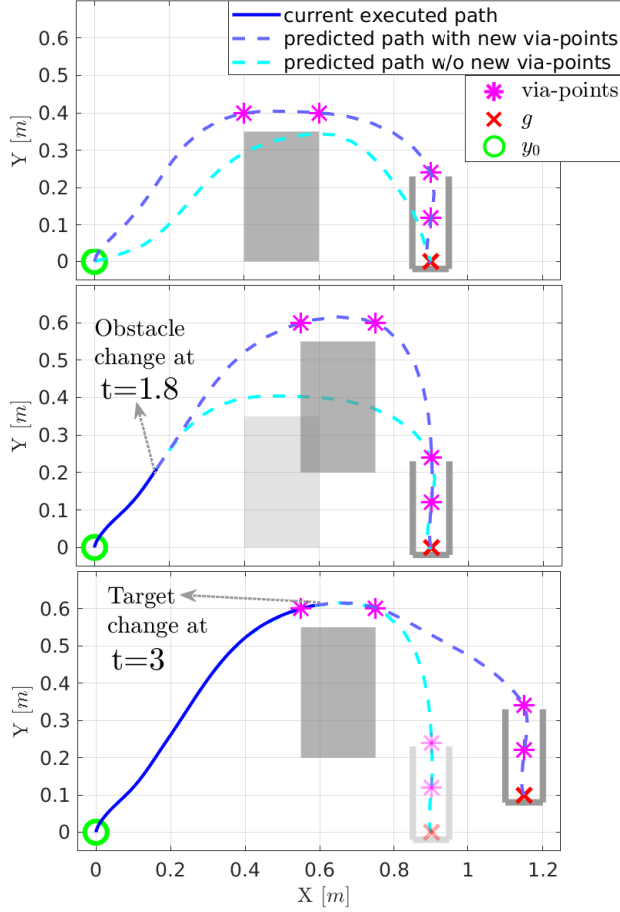


**Fig. 3:** DMP<sup>++</sup> simulation with dynamic via-points. 1st subplot: Initial predicted DMP path (i.e. the one that would be produced) with and w/o the via-points. 2nd subplot: The obstacle is displaced and the current executed DMP path as well as the previous and updated predicted DMP path w/o and with the new via-points is shown. 3rd subplot: The target is displaced.

the one that would be produced) without the via-points plotted with dashed cyan line, and after the adaptation to the via-points with light blue dashed line. At  $t = 1.8$  sec, the obstacle is abruptly displaced (Fig. 3, middle subplot), and the previous predicted DMP path and the new predicted DMP path, based on the updated via-points, are plotted again. The DMP path that has been executed so far is also shown with solid blue line. Finally, at  $t = 3$  sec, the target is abruptly displaced (Fig. 3, bottom subplot). In all simulation snapshots, comparing the cyan with the light blue dashed line, it's obvious that without updating the DMP to the new via-points, either a collision with the obstacle would occur or failure to reach the target without bumping at the boxes's boundaries.

We carried out the same simulation with VMP and plot the final results against the DMP<sup>++</sup> in Fig. 4, where on the top subplot the 2D paths are drawn and on the bottom subplots the velocities and accelerations against the demonstrated ones. It can be observed from the velocities and accelerations that VMP generates more abrupt and higher velocities and accelerations, that differ significantly compared to the demo. This shortcoming is due to the fact that the VMP adaptation

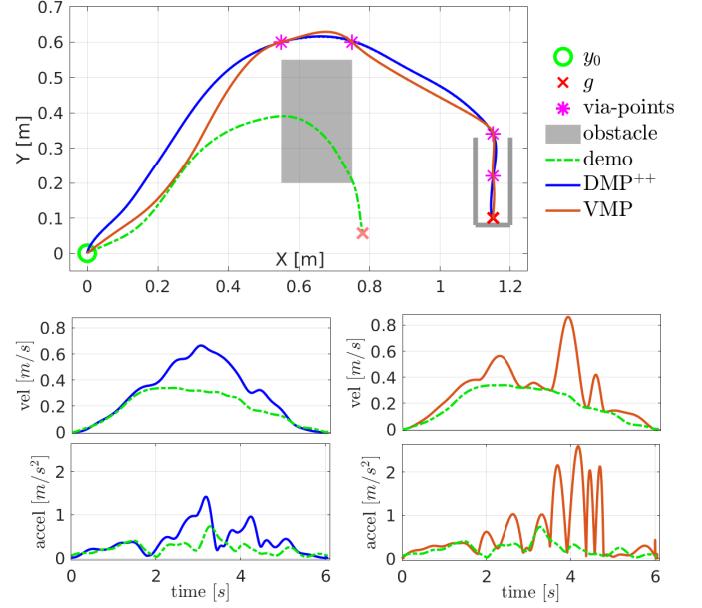


**Fig. 4:** DMP<sup>++</sup> vs VMP. Top plot: 2D paths. Bottom plots: velocities and accelerations.

essentially overrides the demo with the only criterion being the satisfaction of the two currently active via-point constraints. In contrast, DMP<sup>++</sup> performs a global optimization (see (11)) that considers all via-points and adapts in a way as consistent as possible with the demo.

#### D. Adding kinematic inequality constraints

Here we compare with the framework in [24] which uses the DMP formulation [23] with the classical DMP scaling to generate the generalized trajectory  $\{y_d, \dot{y}_d, \ddot{y}_d\}_i$  over a horizon of  $N$  future time-steps which is then optimized to respect kinematic limits like position velocity and acceleration bounds as well as passing from via-points. We show that by modifying the framework from [24] according to Fig. 5, where the DMP with the classical scaling is replaced by DMP<sup>++</sup> we achieve more efficient generalization that accounts also for via-points. Notice that via-points are included both in DMP<sup>++</sup> and in the optimization module of [24] (Fig. 5 brown rectangle) via the respective equality constraints so as to guarantee that the constrained within the kinematic inequality limits trajectory will also pass from the via-points.

Simulation results of a 1 DoF example with two via points and position, velocity and acceleration limits are shown in Fig. 6, where the method proposed in [24] is used to optimize the velocity profile with all relevant parameters chosen as in [24]. To endow the optimizer with greater flexibility in finding feasible solutions we consider the kinematic limits as hard limits (grey dashed lines) and introduce the lower and upper soft limits (magenta dashed lines) within the hard limits. We want to preferably operate within the soft limits and only exceed them if feasibility would be inevitable otherwise [24]. It can be observed that the DMP<sup>++</sup> (blue line) retains the shape of the demonstration (green dash dotted line), even in the presence of kinematic limits and via-points (red asterisks).

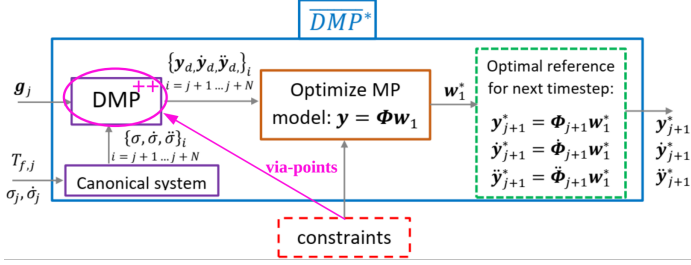


**Fig. 5:** Combination of the proposed spatial generalization with [24] to further impose kinematic inequality constraints. The image is taken from [24], where the differences/additions are highlighted with magenta. DMP<sup>++</sup> replaces the DMP with the classical spatial scaling. Via-points are also considered during the generation of the generalized (unconstrained) trajectory  $y_d$ .

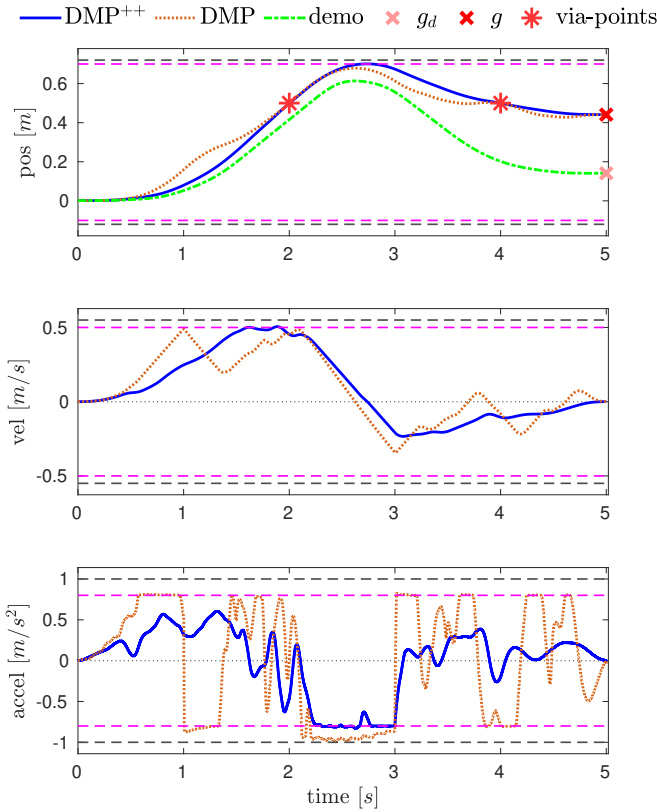


**Fig. 6:** Comparison of the classical DMP spatial generalization against the proposed DMP<sup>++</sup> in combination with [24] to enforce kinematic inequality constraints.

On the other hand, the DMP with the classical scaling (mustard dotted line) can induce large scalings that generate velocities and accelerations that violate considerably the limits, leading to saturation (see the 2nd and 3rd subplots of Fig. 6) and consequently the distortion of the demonstrated shape, as can be observed comparing the mustard with the green trajectory in the first subplot. This distortion would be even more adverse for cases in which scaling is problematic like those presented in Fig. 1, where a feasible solution may even not be found.

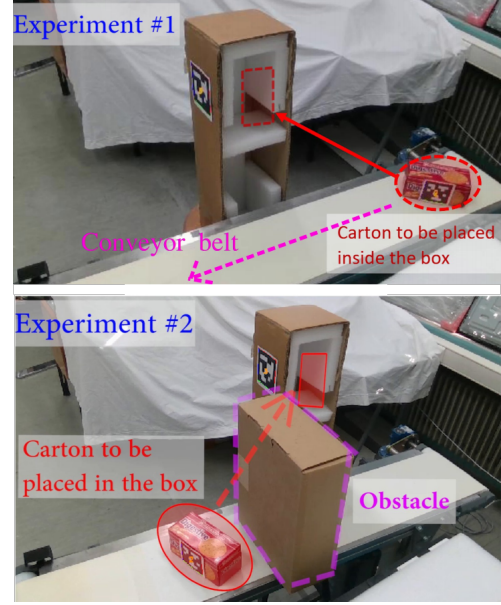


**Fig. 7:** Experimental setup.

## V. EXPERIMENTAL RESULTS

For experimental validation we consider a general scenario that highlights the spatial generalization of DMP<sup>++</sup> and incorporation of dynamic via-points, while also exhibiting the robustness to perturbations, on-line adaptation capabilities and reversibility properties of DMP<sup>++</sup>. Specifically, a robot has to pick a carton from a conveyor belt and insert it inside a box. The pose of the carton and the box are tracked using apriltags with a frame rate of 30 Hz. Two DMP are trained through PbD, one for picking and the second for inserting the carton in the box. To feature the aforementioned properties, we examined the two scenarios depicted in Fig. 7. In the first (top picture), the carton is moving on the conveyor belt and a perturbation of its pose is also introduced by having a human displace it during execution. In the second scenario (bottom picture), an obstacle obstructs the robot from picking the carton. In this scenario two variants are examined: a) introducing a coupling term from a force exerted by a human, who intervenes to guide the robot over the obstacle or b) using via-points, obtained from an apriltag that the human uses to demonstrate a detour around the obstacle. In all experiments, to guarantee that the carton is properly inserted in the box, we specified 5 additional via-points with the same orientation with the carton's target with 3 cm offset between them starting from the target position. Moreover, to test the adaptation to dynamic via-points, in all experiments during the placing of the carton, the target pose of the box (and hence its associated via-points) are altered on the fly.

To carry out these experiments a velocity controlled ur5e robot is used, with 2 ms control cycle, which takes as reference the velocity produced by the DMP transformation system from (1), where  $y$  is either the Cartesian position or for orientation  $y = \log(Q * Q_0)$ . We also add in (1) the coupling term  $u = J_i M_i^{-1} f_i - a_i \ddot{y}_s$ , where  $i \in \{p, o\}$  for position and orientation respectively,  $J_p = I_3$ ,  $J_o = J_\eta^T$  (see (30)),



$M_p = 5$  and  $M_o = 2$  can be interpreted as the desired inertia in (1), with damping  $M_i D$  and stiffness  $M_i K$ ,  $f_i$  is the external force/torque measured by the robot's F/T sensor at its wrist and  $a_i \ddot{y}_s$ , with  $a_i = \sqrt{\min(2 \|f_i\|, 1.0)}$ , is used to mitigate the effect of the feed-forward acceleration  $\ddot{y}_s$  of the DMP whenever the external force/torque is greater than 0.5 N/Nm. This is useful when there is undesired contact or when the human guides physically the robot to alter its trajectory. The DMP weights are updated online according to (12), (14), while  $\epsilon$  was set as in the simulations. The current state constraint in the optimization is set to the actual robot's state. In all cases, the optimization at each control cycle was below 0.8 ms, which is well within the 2ms control cycle of the robot. For the canonical system from (5), we define  $\dot{s}_d = \dot{s}_1 / (1 + a_d \|f_p\|)$ ,  $a_d > 0$ , which is used to enable phase stopping when an external force is applied. For forward execution we set  $s(0) = 0$  and  $\dot{s}(0) = \dot{s}_1 = \frac{1}{T_f}$ , while for reverse (retraction)  $s(0) = 1$  and  $\dot{s}(0) = \dot{s}_1 = -\frac{1}{T_f}$ . Also, for the case that we want the DMP to adapt to actual robot's state, that may change due to external signals (experiment 2 - case (b)), we disable phase stopping, i.e.  $\dot{s}_d = \dot{s}_1$ , as in this case the measured external force is used to adapt the DMP trajectory and is not meant to stop its evolution.

A video with the complete experimental scenarios along with explanations and visualizations can be found at [dropbox.com/s/x482jf6dcx7ybo5/video.mp4](https://dropbox.com/s/x482jf6dcx7ybo5/video.mp4). Indicative results from scenario 1 (Fig. 7, top picture) are plotted in Fig. 8. On the top subplot, it can be observed that continuous changes or even abrupt changes of the target during pick (red line) and place (magenta) are handled smoothly by the proposed DMP (blue and cyan line). On the bottom subplot, the phase variable evolution is plotted, where during placing at  $t \approx 12$  sec, the human holds the robot's end-effector and the exerted force (mustard line) triggers phase stopping, while in the meantime the human displaces the box (top plot, magenta line).

For the second scenario, the results in Fig. 9 demonstrate on the top the adjusted DMP trajectory during the pick (brown line) along the  $x$ -axis, where the maximal deviation from the nominal trajectory (magenta dashed line) occurred. This adaptation required a moderate human force (mustard line) of less than 6 N. On the bottom subplot, the paths for the pick and place are drawn, where for the place the associated via-points are also visualized, from the initial to the finally displaced position of the box. Finally, the same scenario is revisited, only this time the human does not interact physically with the robot. Instead, he uses an apriltag as indicator of the via-points' pose, through which the robot should pass. Results are presented in Fig. 10. where on top, the via-points and the DMP adjusted trajectory along the  $x$ -axis is plotted, and on the bottom, the 3D paths and the via-points are visualized.

## VI. CONCLUSIONS

In this work we presented an improved spatial generalization for DMP, that does not exhibit the shortcomings of other spatial generalization approaches, and moreover enables the incorporation of dynamic via-points. We achieve this by

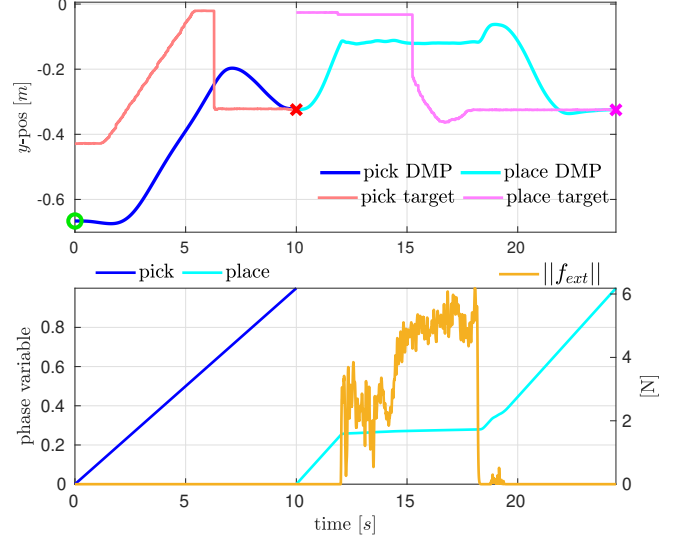


**Fig. 8:** Experiment 1. Top:  $y$  position of the DMP (blue line) for picking the carton (red line) and the DMP (cyan line) for placing the carton in the box (magenta line). Bottom: Phase variable evolution for picking (blue) and for placing (cyan) superimposed with the external force (mustard line).

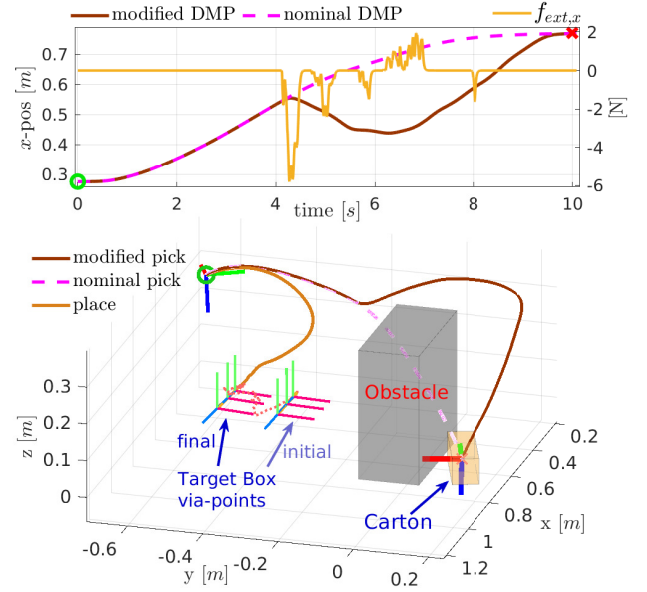


**Fig. 9:** Experiment 2-case a: Adaptation of DMP to external force. Top:  $x$ -position of nominal (dashed magenta line) and the modified DMP (brown line) for picking the carton, superimposed with the applied force (mustard line). Bottom: Cartesian path of the DMP for picking and placing the carton in the box.

proposing an on-line adaptation scheme for the DMP weights, that is shown to solve the problem of minimizing the distance from the learned demonstrated acceleration profile, in order to retain the demonstrated motion pattern, subject to dynamic via-points and initial/final state constraints. Comparative simulations with other SoA methods showcase the advantages of the proposed method. Further validation was carried out via dynamic experimental scenarios.

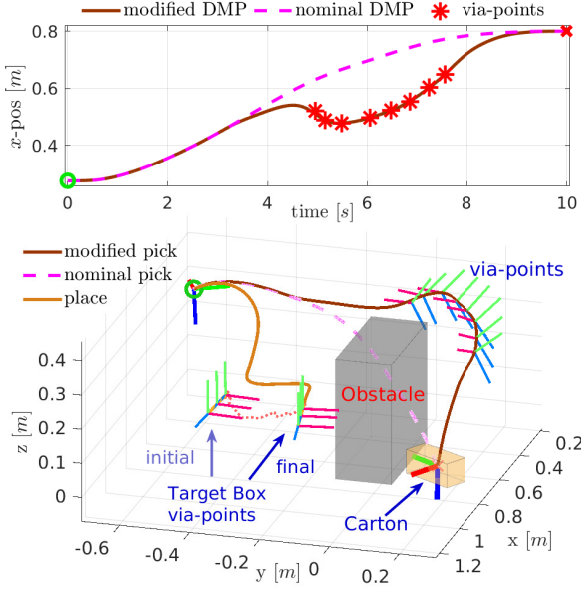


**Fig. 10:** Experiment 2-case b: Adaptation of DMP with via-points. Top:  $x$ -position of nominal (dashed magenta line) and the modified DMP (brown line) for picking the carton. Bottom: Cartesian path of the DMP for picking and placing the carton in the box.

#### APPENDIX A - UNIT QUATERNION PRELIMINARIES

Given a rotation matrix  $\mathbf{R} \in SO(3)$ , an orientation can be expressed in terms of the unit quaternion  $\mathbf{Q} \in \mathbb{S}^3$  as  $\mathbf{Q} = [w \ \mathbf{v}^T]^T = [\cos(\theta_2) \ \sin(\theta_2)\mathbf{k}^T]^T$ , where  $\mathbf{k} \in \mathbb{S}^2$ ,  $\theta_2 = \theta/2$  with  $\theta \in [-\pi, \pi)$  are the equivalent unit axis-angle representation. The quaternion product between the unit quaternions  $\mathbf{Q}_1, \mathbf{Q}_2$  is denoted as  $\mathbf{Q}_1 * \mathbf{Q}_2$ . The inverse of a unit quaternion is equal to its conjugate which is  $\mathbf{Q}^{-1} = \mathbf{Q} = [w \ -\mathbf{v}^T]^T$ . The logarithmic  $\boldsymbol{\eta} = \log(\mathbf{Q})$  and exponential  $\mathbf{Q} = \exp(\boldsymbol{\eta})$  mappings  $\log : \mathbb{S}^3 \rightarrow \mathbb{R}^3$ ,  $\exp : \mathbb{R}^3 \rightarrow \mathbb{S}^3$  respect the manifold's geometry and are defined as follows:

$$\log(\mathbf{Q}) \triangleq \begin{cases} 2 \cos^{-1}(w) \frac{\mathbf{v}}{\|\mathbf{v}\|}, & |w| \neq 1 \\ [0, 0, 0]^T, & \text{otherwise} \end{cases} \quad (19)$$

$$\exp(\boldsymbol{\eta}) \triangleq \begin{cases} [\cos(\|\boldsymbol{\eta}/2\|), \sin(\|\boldsymbol{\eta}/2\|) \frac{\boldsymbol{\eta}^T}{\|\boldsymbol{\eta}\|}]^T, & \|\boldsymbol{\eta}\| \neq 0 \\ [1, 0, 0, 0]^T, & \text{otherwise} \end{cases} \quad (20)$$

It can be found analytically that the relations between the rotational velocity and the derivative of the quaternion logarithm are:

$$\boldsymbol{\omega} = \mathbf{J}_\eta \dot{\boldsymbol{\eta}} \quad (21)$$

$$\dot{\boldsymbol{\eta}} = \mathbf{J}_\eta^\dagger \boldsymbol{\omega} \quad (22)$$

where

$$\mathbf{J}_\eta \triangleq \mathbf{k}\mathbf{k}^T + \frac{\sin(\theta_2) \cos(\theta_2)}{\theta_2} (\mathbf{I}_3 - \mathbf{k}\mathbf{k}^T) + \frac{\sin^2(\theta_2)}{\theta_2} [\mathbf{k}]_\times \quad (23)$$

$$\mathbf{J}_\eta^\dagger = \mathbf{k}\mathbf{k}^T + \frac{\theta_2 \cos(\theta_2)}{\sin(\theta_2)} (\mathbf{I}_3 - \mathbf{k}\mathbf{k}^T) - \theta_2 [\mathbf{k}]_\times \quad (24)$$

where  $[\mathbf{k}]_{\text{times}}$  denotes the skew-symmetric matrix of  $\mathbf{k}$ . For  $\theta = 0$  it can be easily verified that taking the limit of (23), (24) and using L'Hospital's rule we get  $\mathbf{J}_\eta = \mathbf{J}_\eta^\dagger = \mathbf{I}_3$ .

Differentiating (21), (22) we can obtain the relations between the quaternion logarithm second time derivative and the rotational acceleration:

$$\dot{\boldsymbol{\omega}} = \mathbf{J}_\eta \ddot{\boldsymbol{\eta}} + \dot{\mathbf{J}}_\eta \dot{\boldsymbol{\eta}} \quad (25)$$

$$\ddot{\boldsymbol{\eta}} = \mathbf{J}_\eta^\dagger \dot{\boldsymbol{\omega}} + \dot{\mathbf{J}}_\eta^\dagger \boldsymbol{\omega} \quad (26)$$

where

$$\begin{aligned} \dot{\mathbf{J}}_\eta = & \left(1 - \frac{\sin(\theta_2) \cos(\theta_2)}{\theta_2}\right) (\dot{\mathbf{k}}\mathbf{k}^T + \mathbf{k}\dot{\mathbf{k}}^T) + \frac{\sin^2(\theta_2)}{\theta_2} [\dot{\mathbf{k}}]_\times \\ & + \left(\frac{1 - 2\sin^2(\theta_2)}{\theta_2} - \frac{\sin(\theta_2) \cos(\theta_2)}{\theta_2^2}\right) \dot{\theta}_2 (\mathbf{I}_3 - \mathbf{k}\mathbf{k}^T) \\ & + \left(\frac{2\sin(\theta_2) \cos(\theta_2)}{\theta_2} - \frac{\sin^2(\theta)}{\theta_2^2}\right) \dot{\theta}_2 [\mathbf{k}]_\times \end{aligned} \quad (27)$$

$$\begin{aligned} \dot{\mathbf{J}}_\eta^\dagger = & \left(1 - \frac{\theta_2 \cos(\theta_2)}{\sin(\theta_2)}\right) (\dot{\mathbf{k}}\mathbf{k}^T + \mathbf{k}\dot{\mathbf{k}}^T) - \dot{\theta}_2 [\mathbf{k}]_\times - \theta_2 [\dot{\mathbf{k}}]_\times \\ & + \left(\frac{\sin(\theta_2) \cos(\theta_2) - \theta_2}{\sin^2(\theta_2)}\right) \dot{\theta}_2 (\mathbf{I}_3 - \mathbf{k}\mathbf{k}^T) \end{aligned} \quad (28)$$

with  $\dot{\theta}_2 = \frac{1}{2} \mathbf{k}^T \dot{\boldsymbol{\eta}}$  and  $\dot{\mathbf{k}} = \frac{1}{2} \left( \frac{1 - \mathbf{k}\mathbf{k}^T}{\theta_2} \dot{\boldsymbol{\eta}} \right)$ . Taking the limit of (27), (28) for  $\theta = 0$  we have that  $\dot{\mathbf{J}}_\eta = \dot{\mathbf{J}}_\eta^\dagger = \mathbf{0}$ .

Finally, the relations between the Cartesian torque  $\boldsymbol{\tau}$  and its transformation in the quaternion logarithm space  $\boldsymbol{\tau}_\eta$  is given by:

$$\boldsymbol{\tau}_\eta = \mathbf{J}_\eta^T \boldsymbol{\tau} \quad (29)$$

$$\boldsymbol{\tau} = (\mathbf{J}_\eta^\dagger)^T \boldsymbol{\tau}_\eta \quad (30)$$

These mappings follow readily from the preservation of power, i.e. it should hold that  $\boldsymbol{\omega}^T \boldsymbol{\tau} = \dot{\boldsymbol{\eta}}^T \boldsymbol{\tau}_\eta$ .

#### APPENDIX B - RECURSIVE LEAST SQUARES DERIVATIONS

Here we provide some useful results in the form of theorems which facilitate the proof of the update formulas (12), (14) that solve (11). Results in Section 2 from [26] for vectors are here extended for matrices in *Theorems 1, 2* and *5*. *Theorems 1, 2* are used in the proof of *Theorems 3 – 5*, and *Theorems 2 – 5* are employed in the proof for solving (11).

*Theorem 1:* The solution to the problem:

$$\min_{\mathbf{W}} \text{tr}\{(\mathbf{Y} - \mathbf{W}^T \boldsymbol{\Phi})^T \mathbf{R}^{-1} (\mathbf{Y} - \mathbf{W}^T \boldsymbol{\Phi})\} \quad (31)$$

with  $\mathbf{Y} \in \mathbb{R}^{n \times m}$ ,  $\mathbf{W} \in \mathbb{R}^{k \times n}$ ,  $\boldsymbol{\Phi} \in \mathbb{R}^{k \times m}$ ,  $\text{rank}(\boldsymbol{\Phi}) = k$ ,  $\mathbf{R} \in \mathcal{S}_{++}^n$  is given by:

$$\mathbf{W}_0 = \mathbf{P}_0 \boldsymbol{\Phi} \mathbf{R}^{-1} \mathbf{Y}^T \quad (32)$$

$$\mathbf{P}_0 = (\boldsymbol{\Phi} \mathbf{R}^{-1} \boldsymbol{\Phi}^T)^{-1} \quad (33)$$

where  $\mathbf{P}_0 > \mathbf{0}$ .

*Proof:* Taking the derivative of  $f_0$  w.r.t.  $\mathbf{W}$  and solving for  $\mathbf{W}$ , it is straightforward to verify that the solution is indeed given by  $\mathbf{W}_0$ , where  $\mathbf{P} > \mathbf{0}$  since  $\mathbf{R} > \mathbf{0}$  and  $\text{rank}(\boldsymbol{\Phi}) = k$ . ■

*Theorem 2:* The solution to the problem:

$$\min_{\mathbf{W}} f_0(\mathbf{W}) + \text{tr}\{(\mathbf{Z} - \mathbf{W}^T \mathbf{H})^T \mathbf{R}_1^{-1} (\mathbf{Z} - \mathbf{W}^T \mathbf{H})\} \quad (34)$$

with  $f_0(\mathbf{W}) = \text{tr}\{(\mathbf{Y} - \mathbf{W}^T \bar{\Phi})^T \mathbf{R}^{-1}(\mathbf{Y} - \mathbf{W}^T \bar{\Phi})\}$ ,  $\mathbf{Y} \in \mathbb{R}^{n \times m}$ ,  $\mathbf{W} \in \mathbb{R}^{k \times n}$ ,  $\bar{\Phi} \in \mathbb{R}^{k \times m}$ ,  $\text{rank}(\bar{\Phi}) = k$ ,  $\mathbf{R}, \mathbf{R}_1 \in \mathcal{S}_{++}^n$ ,  $\mathbf{Z} \in \mathbb{R}^{n \times l}$ ,  $\mathbf{H} \in \mathbb{R}^{k \times l}$ , can be obtained from the solution  $\mathbf{W}_0$ ,  $\mathbf{P}_0$  of  $\min_{\mathbf{W}} f_0(\mathbf{W})$  as follows:

$$\mathbf{W}_1 = \mathbf{W}_0 + \mathbf{P}_0 \mathbf{H} (\mathbf{R}_1 + \mathbf{H}^T \mathbf{P}_0 \mathbf{H})^{-1} (\mathbf{Z} - \mathbf{W}_0^T \mathbf{H})^T \quad (35)$$

$$\mathbf{P}_1 = \mathbf{P}_0 - \mathbf{P}_0 \mathbf{H} (\mathbf{R}_1 + \mathbf{H}^T \mathbf{P}_0 \mathbf{H})^{-1} \mathbf{H}^T \mathbf{P}_0 \quad (36)$$

$$\mathbf{P}_1^{-1} = \mathbf{P}_0 + \mathbf{H} \mathbf{R}_1^{-1} \mathbf{H}^T \quad (37)$$

where  $\mathbf{P}_1 > \mathbf{0}$ .

*Proof:* We can rewrite the cost function in (34) as

$$\text{tr}\{(\bar{\mathbf{Y}} - \mathbf{W}^T \bar{\Phi})^T \bar{\mathbf{R}}^{-1}(\bar{\mathbf{Y}} - \mathbf{W}^T \bar{\Phi})\}$$

with

$$\bar{\mathbf{Y}} = [\mathbf{Y}^T \ \mathbf{Z}^T]^T, \ \bar{\Phi} = [\Phi^T \ \mathbf{H}^T]^T, \ \bar{\mathbf{R}} = \text{blkdiag}(\mathbf{R}, \mathbf{R}_1)$$

and apply the result of *Theorem 1* to get:

$$\mathbf{W} = \mathbf{P}_1^{-1} \bar{\Phi} \bar{\mathbf{R}}^{-1} \bar{\mathbf{Y}}^T = \mathbf{P}_1^{-1} (\Phi \mathbf{R}^{-1} \mathbf{Y}^T + \mathbf{H} \mathbf{R}_1^{-1} \mathbf{Z}^T) \quad (38)$$

where  $\mathbf{P}_1^{-1} = \bar{\Phi} \bar{\mathbf{R}}^{-1} \bar{\Phi}^T = (\mathbf{P}_0^{-1} + \mathbf{H} \mathbf{R}_1^{-1} \mathbf{H}^T)$  with  $\mathbf{P}_0^{-1} = \Phi \mathbf{R}^{-1} \Phi^T$ . It follows that  $\mathbf{P}_1^{-1} > \mathbf{0}$ , since  $\mathbf{P}_0^{-1} > \mathbf{0}$ , due to  $\mathbf{R} > \mathbf{0}$  and  $\text{rank}(\Phi) = k$ , and  $\mathbf{H} \mathbf{R}_1^{-1} \mathbf{H}^T \geq \mathbf{0}$ . Applying the matrix inversion lemma it follows that  $\mathbf{P}_1$  is indeed given by (36) and substituting it in (38) we get:

$$\begin{aligned} \mathbf{W} &= \mathbf{W}_0 - \mathbf{P}_0 \mathbf{H} (\mathbf{R}_1 + \mathbf{H}^T \mathbf{P}_0 \mathbf{H})^{-1} (\mathbf{W}_0^T \mathbf{H})^T + \\ &\quad (\mathbf{P}_0 - \mathbf{P}_0 \mathbf{H} (\mathbf{R}_1 + \mathbf{H}^T \mathbf{P}_0 \mathbf{H})^{-1} \mathbf{H}^T \mathbf{P}_0) \mathbf{H} \mathbf{R}_1^{-1} \mathbf{Z}^T \end{aligned} \quad (39)$$

where  $\mathbf{W}_0 = \mathbf{P}_0 \Phi \mathbf{R}^{-1} \mathbf{Y}^T$ ,  $\mathbf{P}_0 = (\Phi \mathbf{R}^{-1} \Phi^T)^{-1}$  is indeed the solution of  $\min_{\mathbf{W}} f_0(\mathbf{W})$  based on *Theorem 1*. We can further process the last term in (39), i.e.:

$$\begin{aligned} &(\mathbf{P}_0 - \mathbf{P}_0 \mathbf{H} (\mathbf{R}_1 + \mathbf{H}^T \mathbf{P}_0 \mathbf{H})^{-1} \mathbf{H}^T \mathbf{P}_0) \mathbf{H} \mathbf{R}_1^{-1} \mathbf{Z}^T \\ &= (\mathbf{P}_0 \mathbf{H} - \mathbf{P}_0 \mathbf{H} (\mathbf{R}_1 + \mathbf{H}^T \mathbf{P}_0 \mathbf{H})^{-1} \mathbf{H}^T \mathbf{P}_0 \mathbf{H}) \mathbf{R}_1^{-1} \mathbf{Z}^T \\ &= \mathbf{P}_0 \mathbf{H} (\mathbf{I}_k - (\mathbf{R}_1 + \mathbf{H}^T \mathbf{P}_0 \mathbf{H})^{-1} (\pm \mathbf{R}_1 + \mathbf{H}^T \mathbf{P}_0 \mathbf{H})) \mathbf{R}_1^{-1} \mathbf{Z}^T \\ &= \mathbf{P}_0 \mathbf{H} (\mathbf{R}_1 + \mathbf{H}^T \mathbf{P}_0 \mathbf{H})^{-1} \mathbf{Z}^T \end{aligned} \quad (40)$$

and substituting it back to (39) we arrive at the solution given by (35). ■

*Theorem 3:* Problem (34) is equivalent to the problem

$$\min_{\mathbf{W}} \text{tr}\{(\mathbf{W} - \mathbf{W}_0) \mathbf{P}_0^{-1} (\mathbf{W} - \mathbf{W}_0)^T\} + \quad (41)$$

$$\text{tr}\{(\mathbf{Z} - \mathbf{W}^T \mathbf{H})^T \mathbf{R}_1^{-1} (\mathbf{Z} - \mathbf{W}^T \mathbf{H})\} \quad (42)$$

where  $\mathbf{W}_0$ ,  $\mathbf{P}_0$  are the solution to  $\min_{\mathbf{W}} f_0(\mathbf{W})$ .

*Proof:* Taking the gradient and solving w.r.t.  $\mathbf{W}$  we can readily obtain (38) after which the same analysis as in the proof of *Theorem 2* follows. ■

*Theorem 4:* The optimization problem

$$\min_{\mathbf{W}} f_0(\mathbf{W}) \quad (43)$$

$$\text{s.t. } \mathbf{W}^T \mathbf{H} = \mathbf{Z}$$

with  $f_0(\mathbf{W}) = \text{tr}\{(\mathbf{Y} - \mathbf{W}^T \bar{\Phi})^T \mathbf{R}^{-1}(\mathbf{Y} - \mathbf{W}^T \bar{\Phi})\}$ ,  $\mathbf{Y} \in \mathbb{R}^{n \times m}$ ,  $\mathbf{W} \in \mathbb{R}^{k \times n}$ ,  $\bar{\Phi} \in \mathbb{R}^{k \times m}$ ,  $\text{rank}(\bar{\Phi}) = k$ ,  $\mathbf{R} \in \mathcal{S}_{++}^n$ ,  $\mathbf{Z} \in \mathbb{R}^{n \times l}$ ,  $\mathbf{H} \in \mathbb{R}^{k \times l}$ ,  $\text{rank}(\mathbf{H}) = l \leq k$ , is equivalent to the problem:

$$\min_{\mathbf{W}} f_0(\mathbf{W}) + \text{tr}\{(\mathbf{Z} - \mathbf{W}^T \mathbf{H})^T \mathbf{R}_\epsilon^{-1} (\mathbf{Z} - \mathbf{W}^T \mathbf{H})\} \quad (44)$$

for  $\mathbf{R}_\epsilon \rightarrow \mathbf{0}^+$ .

*Proof:* To find the solution of (43) we introduce the Language multipliers  $\mathbf{V} \in \mathbb{R}^{n \times l}$  and form the Lagrangian  $L(\mathbf{W}, \mathbf{V}) = f_0(\mathbf{W}) + 2\text{tr}\{\mathbf{V}^T (\mathbf{W}^T \mathbf{H} - \mathbf{Z})\}$ . The KKT conditions are:

$$\frac{\partial L}{\partial \mathbf{W}} = -\bar{\Phi}(\mathbf{Y} - \mathbf{W}^T \bar{\Phi})^T + \mathbf{H} \mathbf{V} = \mathbf{0} \quad (45)$$

$$\frac{\partial L}{\partial \mathbf{V}} = \mathbf{H}^T \mathbf{W} - \mathbf{Z}^T = \mathbf{0} \quad (46)$$

Solving (45) for  $\mathbf{W}$  we get:

$$\mathbf{W} = \mathbf{W}_0 - \mathbf{P}_0 \mathbf{H} \mathbf{V} \quad (47)$$

where  $\mathbf{W}_0 = \mathbf{P}_0 \bar{\Phi} \mathbf{Y}^T$ ,  $\mathbf{P}_0 = (\bar{\Phi} \mathbf{R}^{-1} \bar{\Phi}^T)^{-1}$  which is indeed invertible since  $\text{rank}(\bar{\Phi}) = k$ . Since  $\mathbf{P}_0$  is invertible and  $\text{rank}(\mathbf{H}) = l$ , i.e. has full column rank, we can substitute (47) in (46) to solve for  $\mathbf{V}$ :

$$\mathbf{V} = -(\mathbf{H}^T \mathbf{P}_0 \mathbf{H})^{-1} (\mathbf{Z} - \mathbf{W}_0^T \mathbf{H})^T$$

Substituting the last equation in (47), we obtain the solution:

$$\mathbf{W}_1 = \mathbf{W}_0 + \mathbf{P}_0 \mathbf{H} (\mathbf{H}^T \mathbf{P}_0 \mathbf{H})^{-1} (\mathbf{Z} - \mathbf{W}_0^T \mathbf{H})^T \quad (48)$$

Turning our attention to problem (44) we can apply the result of *Theorem 2* and notice that for  $\mathbf{R}_1 = \mathbf{R}_\epsilon \rightarrow \mathbf{0}^+$  we get indeed the same solution as in (48). ■

*Theorem 5:* Given the solution  $\mathbf{W}_1$ ,  $\mathbf{P}_1$  of the problem

$$\min_{\mathbf{W}} f_0(\mathbf{W}) + \text{tr}\{(\mathbf{Z} - \mathbf{W}^T \mathbf{H})^T \mathbf{R}_1^{-1} (\mathbf{Z} - \mathbf{W}^T \mathbf{H})\} \quad (49)$$

with  $f_0(\mathbf{W}) = \text{tr}\{(\mathbf{Y} - \mathbf{W}^T \bar{\Phi})^T \mathbf{R}^{-1}(\mathbf{Y} - \mathbf{W}^T \bar{\Phi})\}$ ,  $\mathbf{Y} \in \mathbb{R}^{n \times m}$ ,  $\mathbf{W} \in \mathbb{R}^{k \times n}$ ,  $\bar{\Phi} \in \mathbb{R}^{k \times m}$ ,  $\text{rank}(\bar{\Phi}) = k$ ,  $\mathbf{R}, \mathbf{R}_1 \in \mathcal{S}_{++}^n$ ,  $\mathbf{Z} \in \mathbb{R}^{n \times l}$ ,  $\mathbf{H} \in \mathbb{R}^{k \times l}$ , the solution to the problem:

$$\min_{\mathbf{W}} f_0(\mathbf{W}) \quad (50)$$

can be calculated as:

$$\hat{\mathbf{W}}_0 = \mathbf{W}_1 + \mathbf{P}_1 \mathbf{H} (-\mathbf{R}_1 + \mathbf{H}^T \mathbf{P}_1 \mathbf{H})^{-1} (\mathbf{Z} - \mathbf{W}_1^T \mathbf{H})^T \quad (51)$$

$$\hat{\mathbf{P}}_0 = \mathbf{P}_1 - \mathbf{P}_1 \mathbf{H} (-\mathbf{R}_1 + \mathbf{H}^T \mathbf{P}_1 \mathbf{H})^{-1} \mathbf{H}^T \mathbf{P}_1 \quad (52)$$

$$\hat{\mathbf{P}}_0^{-1} = \mathbf{P}_1^{-1} - \mathbf{H} \mathbf{R}_1^{-1} \mathbf{H}^T \quad (53)$$

where  $\hat{\mathbf{P}}_0 > \mathbf{0}$ .

*Proof:* Denoting

$$f_1(\mathbf{W}) = f_0(\mathbf{W}) + \text{tr}\{(\mathbf{Z} - \mathbf{W}^T \mathbf{H})^T \mathbf{R}_1^{-1} (\mathbf{Z} - \mathbf{W}^T \mathbf{H})\}$$

it follows that

$$f_0(\mathbf{W}) = f_1(\mathbf{W}) - \text{tr}\{(\mathbf{Z} - \mathbf{W}^T \mathbf{H})^T \mathbf{R}_1^{-1} (\mathbf{Z} - \mathbf{W}^T \mathbf{H})\}$$

We can rewrite  $f_1(\mathbf{W})$  as:

$$f_1(\mathbf{W}) = \text{tr}\{(\bar{\mathbf{Y}} - \mathbf{W}^T \bar{\Phi})^T \bar{\mathbf{R}}^{-1}(\bar{\mathbf{Y}} - \mathbf{W}^T \bar{\Phi})\}$$

with

$$\bar{\mathbf{Y}} = [\mathbf{Y}^T \ \mathbf{Z}^T]^T, \ \bar{\Phi} = [\Phi^T \ \mathbf{H}^T]^T, \ \bar{\mathbf{R}} = \text{blkdiag}(\mathbf{R}, \mathbf{R}_1)$$

Minimizing  $f_0(\mathbf{W})$  we have:

$$\begin{aligned} \frac{\partial f_0}{\partial \mathbf{W}} &= \frac{\partial (f_1(\mathbf{W}) - \text{tr}\{(\mathbf{Z} - \mathbf{W}^T \mathbf{H})^T \mathbf{R}_1^{-1} (\mathbf{Z} - \mathbf{W}^T \mathbf{H})\})}{\partial \mathbf{W}} = \mathbf{0} \\ (\mathbf{P}_1^{-1} - \mathbf{H} \mathbf{R}_1^{-1} \mathbf{H}^T) \mathbf{W} &= (\bar{\Phi} \bar{\mathbf{R}}^{-1} \bar{\mathbf{Y}}^T - \mathbf{H} \mathbf{R}_1^{-1} \mathbf{Z}^T) \end{aligned} \quad (54)$$

where  $P_1^{-1} = \bar{\Phi} \bar{R}^{-1} \bar{\Phi}^T = P_0^{-1} + H R_1^{-1} H^T$  and  $P_0^{-1} = \Phi R^{-1} \Phi^T$ . Since  $R > 0$  and  $\text{rank}(\Phi) = k$  it follows that  $P_0^{-1} > 0$  which also entails that  $P_1^{-1} > 0$  as  $R_1 > 0$  and  $H R_1^{-1} H^T \geq 0$ . Notice also that  $(P_1^{-1} - H R_1^{-1} H^T) = P_0^{-1}$  hence we can invert it in (54) to get:

$$W = (P_1^{-1} - H R_1^{-1} H^T)^{-1} (\bar{\Phi} \bar{R}^{-1} \bar{Y}^T + H(-R_1^{-1}) Z^T)$$

Applying the matrix inversion lemma we have:

$$W = W_1 - P_1 H (-R_1 + H^T P_1 H)^{-1} (W_1^T H)^T + (P_1 - P_1 H (-R_1 + H^T P_1 H)^{-1} H^T P_1) H (-R_1^{-1}) Z^T \quad (55)$$

where  $W_1 = P_1 \bar{\Phi} \bar{R}^{-1} \bar{Y}^T$ ,  $P_1 = (\bar{\Phi} \bar{R}^{-1} \bar{\Phi}^T)^{-1}$  is indeed the solution of  $\min_W f_1(W)$  based on *Theorem 1*. Notice that  $-R_1 + H^T P_1 H$  is in fact negative definite, hence it is invertible. To prove so, consider the following matrix:

$$M = \begin{bmatrix} P_1^{-1} & H \\ H^T & R_1 \end{bmatrix}$$

Since  $P_1^{-1} > 0$  and the Schur complement of  $M$  w.r.t. the upper left block matrix is  $P_1^{-1} - H R_1^{-1} H^T = P_0^{-1} > 0$  it follows that  $M > 0$  [27]. Therefore, as  $R_1 > 0$  and  $M > 0$  it should also hold that the Schur complement of  $M$  w.r.t. the lower right block matrix should be positive definite, i.e.:

$$R_1^{-1} - H^T P_1 H > 0 \Rightarrow -R_1^{-1} + H^T P_1 H < 0$$

We can further process the last term in (55) similar to the analysis in (40) to find that:

$$(P_1 - P_1 H (-R_1 + H^T P_1 H)^{-1} H^T P_1) H (-R_1^{-1}) Z^T = P_1 H (-R_1 + H^T P_1 H)^{-1} Z^T$$

and substituting the last in (55) we obtain the result given by (51). Finally, having already established that  $P_1 > 0$  and  $-R_1^{-1} + H^T P_1 H < 0$  it follows that  $-P_1 H (-R_1 + H^T P_1 H)^{-1} H^T P_1 \geq 0$  hence  $\hat{P}_0 > 0$ . ■

#### DECLARATIONS

No funding was received for conducting this work and there isn't any kind of conflict of interest.

#### REFERENCES

- [1] A. J. Ijspeert, J. Nakanishi, H. Hoffmann, P. Pastor, and S. Schaal, "Dynamical movement primitives: Learning attractor models for motor behaviors," *Neural Comput.*, vol. 25, no. 2, pp. 328–373, Feb 2013.
- [2] P. Pastor, M. Kalakrishnan, F. Meier, F. Stulp, J. Buchli, E. Theodorou, and S. Schaal, "From dynamic movement primitives to associative skill memories," *Robotics and Autonomous Systems*, vol. 61, no. 4, pp. 351–361, 2013, models and Technologies for Multi-modal Skill Training. [Online]. Available: <https://www.sciencedirect.com/science/article/pii/S0921889012001716>
- [3] P. Pastor, L. Righetti, M. Kalakrishnan, and S. Schaal, "Online movement adaptation based on previous sensor experiences," in *2011 IEEE/RSJ International Conference on Intelligent Robots and Systems*, Sept 2011, pp. 365–371.
- [4] A. Ude, A. Gams, T. Asfour, and J. Morimoto, "Task-specific generalization of discrete and periodic dynamic movement primitives," *IEEE Transactions on Robotics*, vol. 26, no. 5, pp. 800–815, 2010.
- [5] J. Umlauf, D. Sieber, and S. Hirche, "Dynamic movement primitives for cooperative manipulation and synchronized motions," in *2014 IEEE International Conference on Robotics and Automation (ICRA)*, 2014, pp. 766–771.
- [6] K. Mülling, J. Kober, O. Kroemer, and J. Peters, "Learning to select and generalize striking movements in robot table tennis," *The International Journal of Robotics Research*, vol. 32, pp. 263–279, 03 2013.

- [7] A. Gams, T. Petric, B. Nemec, and A. Ude, "Learning and adaptation of periodic motion primitives based on force feedback and human coaching interaction," in *2014 IEEE-RAS International Conference on Humanoid Robots*, Nov 2014, pp. 166–171.
- [8] A. Billard, S. Calinon, R. Dillmann, and S. Schaal, *Robot Programming by Demonstration*. Berlin, Heidelberg: Springer Berlin Heidelberg, 2008, pp. 1371–1394.
- [9] H. Hoffmann, P. Pastor, D. Park, and S. Schaal, "Biologically-inspired dynamical systems for movement generation: Automatic real-time goal adaptation and obstacle avoidance," in *2009 IEEE International Conference on Robotics and Automation*, 2009, pp. 2587–2592.
- [10] M. Ginesi, N. Sansonetto, and P. Fiorini, "Overcoming some drawbacks of dynamic movement primitives," *Robotics and Autonomous Systems*, vol. 144, p. 103844, 2021. [Online]. Available: <https://www.sciencedirect.com/science/article/pii/S0921889021001299>
- [11] L. Koutras and Z. Doulgeri, "A novel dmp formulation for global and frame independent spatial scaling in the task space," in *2020 29th IEEE International Conference on Robot and Human Interactive Communication (RO-MAN)*, 2020, pp. 727–732.
- [12] A. D. Dragan, K. Muelling, J. Andrew Bagnell, and S. S. Srinivasa, "Movement primitives via optimization," in *2015 IEEE International Conference on Robotics and Automation (ICRA)*, 2015, pp. 2339–2346.
- [13] Y. Zhou, J. Gao, and T. Asfour, "Learning via-point movement primitives with inter- and extrapolation capabilities," in *2019 IEEE/RSJ International Conference on Intelligent Robots and Systems (IROS)*, 2019, pp. 4301–4308.
- [14] S. Mghames, M. Hanheide, and A. Ghalamzan E., "Interactive movement primitives: Planning to push occluding pieces for fruit picking," in *2020 IEEE/RSJ International Conference on Intelligent Robots and Systems (IROS)*, 2020, pp. 2616–2623.
- [15] C. Cardoso, L. Jamone, and A. Bernardino, "A novel approach to dynamic movement imitation based on quadratic programming," in *2015 IEEE International Conference on Robotics and Automation (ICRA)*, 2015, pp. 906–911.
- [16] J.-J. Kim, S.-Y. Park, and J.-J. Lee, "Adaptability improvement of learning from demonstration with sequential quadratic programming for motion planning," in *2015 IEEE International Conference on Advanced Intelligent Mechatronics (AIM)*, 2015, pp. 1032–1037.
- [17] G. Maeda, M. Ewerton, R. Lioutikov, H. B. Amor, J. Peters, and G. Neumann, "Learning interaction for collaborative tasks with probabilistic movement primitives," in *2014 IEEE-RAS International Conference on Humanoid Robots*, Nov 2014, pp. 527–534.
- [18] G. J. Maeda, G. Neumann, M. Ewerton, R. Lioutikov, O. Kroemer, and J. Peters, "Probabilistic movement primitives for coordination of multiple human–robot collaborative tasks," *Autonomous Robots*, vol. 41, no. 3, pp. 593–612, Mar 2017. [Online]. Available: <https://doi.org/10.1007/s10514-016-9556-2>
- [19] R. Weitschat and H. Aschemann, "Safe and efficient human–robot collaboration part ii: Optimal generalized human-in-the-loop real-time motion generation," *IEEE Robotics and Automation Letters*, vol. 3, no. 4, pp. 3781–3788, 2018.
- [20] A. Paraschos, C. Daniel, J. R. Peters, and G. Neumann, "Probabilistic movement primitives," in *Advances in Neural Information Processing Systems 26*, C. J. C. Burges, L. Bottou, M. Welling, Z. Ghahramani, and K. Q. Weinberger, Eds. Curran Associates, Inc., 2013, pp. 2616–2624. [Online]. Available: <http://papers.nips.cc/paper/5177-probabilistic-movement-primitives.pdf>
- [21] A. Paraschos, C. Daniel, J. Peters, and G. Neumann, "Using probabilistic movement primitives in robotics," *Auton. Robots*, vol. 42, no. 3, p. 529–551, Mar. 2018. [Online]. Available: <https://doi.org/10.1007/s10514-017-9648-7>
- [22] Y. Huang, L. Roza, J. Silvério, and D. G. Caldwell, "Kernelized movement primitives," *The International Journal of Robotics Research*, vol. 38, no. 7, pp. 833–852, 2019.
- [23] A. Sidiropoulos and Z. Doulgeri, "A reversible dynamic movement primitive formulation," in *2021 IEEE International Conference on Robotics and Automation (ICRA)*, 2021, pp. 3147–3153.
- [24] A. Sidiropoulos, D. Papageorgiou, and Z. Doulgeri, "A novel framework for generalizing dynamic movement primitives under kinematic constraints," *Autonomous Robots*, Oct 2022. [Online]. Available: <https://doi.org/10.1007/s10514-022-10067-4>
- [25] R. Wang, Y. Wu, W. L. Chan, and K. P. Tee, "Dynamic movement primitives plus: For enhanced reproduction quality and efficient trajectory modification using truncated kernels and local biases," in *2016 IEEE/RSJ International Conference on Intelligent Robots and Systems (IROS)*, 2016, pp. 3765–3771.



- [26] T. Kailath, A. Sayed, and B. Hassibi, *Linear Estimation*, ser. Prentice-Hall information and system sciences series. Prentice Hall, 2000. [Online]. Available: <https://books.google.gr/books?id=zNJFAQAIAAJ>
- [27] G. Strang, *Linear algebra and its applications*. Belmont, CA: Thomson, Brooks/Cole, 2006.